ACS APPLIED MATERIALS & INTERFACES

Research Article

www.acsami.org

Highly Transparent Dual-Sensitized Titanium Dioxide Nanotube Arrays for Spontaneous Solar Water Splitting Tandem Configuration

Kahee Shin and Jong Hyeok Park*

Department of Chemical and Biomolecular Engineering, Yonsei University, 50 Yonsei-ro, Seodaemun-gu, Seoul 120-749, Republic of Korea

Supporting Information

ABSTRACT: Vertically aligned one-dimensional (1D) titanium dioxide (TiO_2) arrays on transparent conducting oxide (TCO) substrates, which can act as host electron transport materials for low bandgap materials, were synthesized via a hydrothermal reaction combined with a controlled chemical etching process. By controlling the chemical etching conditions, we can maximize the light transmission properties of the 1D TiO_2 arrays, which is beneficial for the front electrode in photoelectrochemical (PEC) tandem configurations. As a result, dual sensitization to form 1D TiO_2@CdS@CdSe (CdS and CdSe coated 1D TiO_2) results in excellent photocurrent density, as well as transparency, and the resulting material is able to pass unabsorbed photons through the front electrode into the rear bias solar cell. Owing to the improved light transmission in combination with the increased specific surface area of the obtained 1D TiO_2 arrays from the controlled etching process, a high-efficiency PEC tandem device with ~2.1% was successfully fabricated for unassisted hydrogen evolution. Efficient PEC tandem device was fabricated for unassisted solar hydrogen generation using highly transparent composite electrode composed of dual sensitization to form 1D TiO_2@CdS@CdSe.

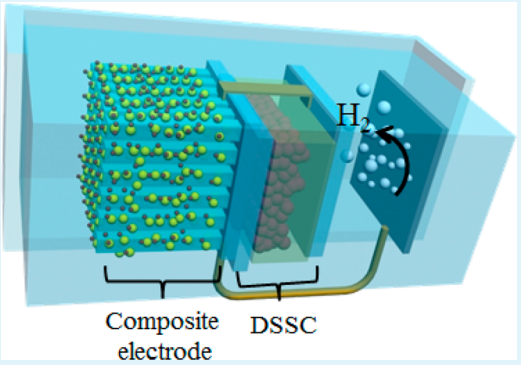

KEYWORDS: *spontaneous hydrogen evolution, water splitting, tandem cell, TiO_2 nanotube*

INTRODUCTION

Since Fujishima and Honda's[1] report on the photocatalytic functionality of TiO_2 for solar water splitting, TiO_2 has been considered one of the most promising photoactive materials due to its remarkable stability, low cost, and strong oxidative properties. During the four decades following this report, various photoelectrochemical (PEC) water splitting systems have been reported using oxide semiconductors with relatively small bandgaps, such as WO_3, $BiVO_4$, and Fe_2O_3. Although these PEC materials showed remarkable photocurrent densities and solar-to-hydrogen conversion efficiencies, they could not achieve devices capable of spontaneous gas evolution (without extra bias) with a high efficiency. To overcome this drawback, various tandem configurations that combine a front metal oxide cell with a rear solar cell have been investigated. In these tandem configurations, the front photoelectrodes were composed of a material with a bandgap of 2.2−2.5 eV, which use a limited portion of the solar spectrum. This causes a serious photocurrent mismatch with the rear solar cells. To increase the light harvesting of the front cell, a thicker photoelectrode could be adapted. However, such an approach would cause an abrupt decrease in the performance of the rear solar cells due to the poor transparency. Consequently, it remains challenging to synthesize a photoanode that exhibits not only a high photocurrent density but also a high transparency for tandem cells.

Recently, the nanoarchitecturing of TiO_2 has been widely used, especially within the photocatalytic area, because of its enlarged surface area while maintaining its original properties.[2,3] Among the various nanostructures, one-dimensional (1D) TiO_2 nanostructures, including nanotubes, nanowires and nanorods, have attracted considerable attention for PEC cells because they can provide an additional advantage of an undisturbed electron transport pathway.[3−5] Various synthetic routes have been proposed to synthesize 1D nanostructures, including the sol−gel method[6] and the vapor−liquid−solid (VLS) method.[7] Unfortunately, it is challenging to form 1D nanorods via these synthetic routes, which are well-aligned and perpendicular to the transparent conductive oxide (TCO) substrate for tandem configurations. Therefore, many research groups have focused on developing facile synthesis methods for single-crystalline 1D TiO_2 nanorod arrays directly grown on TCO substrates (e.g., indium tin oxide (ITO) glass or F-doped tin oxide (FTO) glass)[8,9] However, the bandgap of TiO_2 is still approximately 3.2 eV, which is too large to absorb the visible or near-infrared region of solar light. For this reason, several research groups have focused on modifying the bandgap of TiO_2 using nanocomposites with low bandgap materials such as CdS, CdSe, and PbS.[10−18] Low bandgap material-sensitized

Received: May 25, 2015
Accepted: August 4, 2015
Published: August 4, 2015

DOI: 10.1021/acsami.5b04521
ACS Appl. Mater. Interfaces 2015, 7, 18429−18434

TiO_2 nanostructures are able to extend the light absorption into the visible light region and in turn improve its photoelectrochemical response. However, the interface between 1D TiO_2 and nanoparticles of low bandgap materials was not solid, and thereby, charge transport process and electrochemical reaction occurring in parallel at the triple junction interface (1D TiO_2/low band nanoparticles/electrolyte) constitute one of the major limitations for further improvement of photoelectrochemical response. Reaching higher water splitting efficiencies necessitates gaining a better 1D TiO_2 nanostructure for better triple interface, which will essentially lead to the development of new solutions for PEC systems.

In this study, to synthesize front photoanodes with both high transparency and high photocurrent density for tandem configurations, we prepared dual-sensitized TiO_2 nanotube arrays on FTO substrates. First, from the application of the hydrothermal synthetic method, followed by a tailored chemical etching process, the TiO_2 nanostructure and its optical properties were manipulated. Second, a controlled coating of CdS and CdSe nanoparticles on the TiO_2 surface was conducted by electrodeposition not only to increase its photoelectrochemical response but also to maintain its high transparency (Figure 1a). We demonstrate that the CdS and CdSe coated 1D TiO_2 nanotube arrays (TiO_2 nanotube arrays@CdS@CdSe) composite material is highly suitable for unassisted photoelectrochemical hydrogen generation devices when in tandem with dye-sensitized solar cells, as shown in Figure 1b.

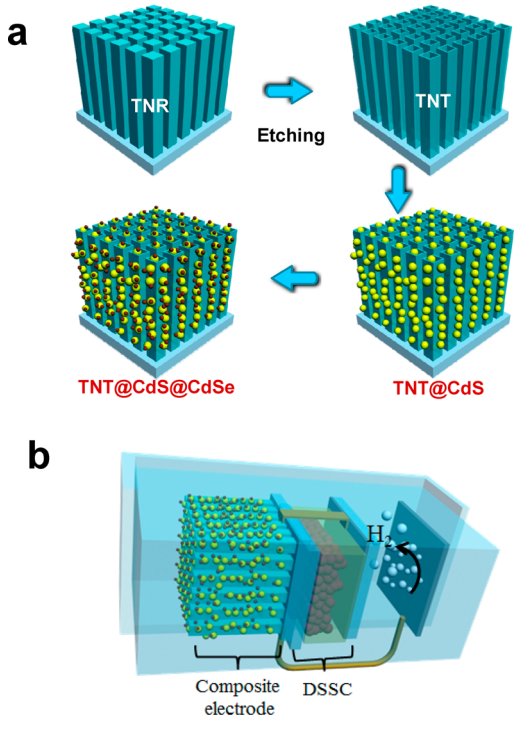

Figure 1. Schematic diagram of (a) the synthesis of CdS/CdSe codeposited TiO_2 nanotube arrays and (b) the tandem device for the hydrogen generation.

EXPERIMENTAL SECTION

Synthesis of TiO_2 Nanorod Arrays on FTO Substrate. The TiO_2 nanorod arrays on a FTO substrate were fabricated using the hydrothermal method.[9] The fluorine-doped tin oxide (SnO_2:F, FTO) glass substrate was cleaned by ultrasonicating in an ethanol and acetone mixture (volumetric ratio of 1:1) for 5 min, followed by rinsing with ethanol and drying with air gas. In a typical synthesis, 20 mL of deionized (DI) water was mixed with 20 mL of concentrated hydrochloric acid (35.0−37.0% by weight) and 0.5 mL of titanium butoxide (97%, Aldrich) in a Teflon-lined autoclave (63 mL). The substrates were placed in the Teflon liner with the conducting side facing down. Then, the solutions were heated at 150 °C for 5 h. After the reaction period, the autoclave was cooled under flowing tap water for 15 min. Then, the samples were rinsed with DI water and dried at room temperature in ambient air.

Transformation of TiO_2 Nanorods into Nanotubes by Chemical Etching. The TiO_2 nanotube arrays were produced from TiO_2 nanorods synthesized by chemical etching using 0.17 M HCl mixed with a 0.20 M HF aqueous solution.[19] The TiO_2 nanorod sample (1.5 × 1.5 cm^2) was immersed in 75 mL of the etching solution and was maintained at 95 °C in an oven for 1−5 h. The sample was rinsed with DI water and dried in ambient air.

Electrodeposition of CdS Nanoparticles. The synthesis of CdS nanoparticles was performed by electrodeposition. An aqueous solution of 0.2 M $CdCl_2$ (>99.0%, Fluka) and 0.05 M $Na_2S_2O_3$ (95%, Samchun), with the pH controlled at ∼2.1 using 1 N HCl, was prepared as a precursor solution. The chemically etched TiO_2 nanotube array sample was immersed in the heated precursor solution at 50 °C, and −0.65 V vs standard calomel electrode (SCE) was applied for 500, 1000, and 1500 s. After electrodeposition, the sample was rinsed with DI water, dried at room temperature, and sintered at 300 °C for 30 min in air.

Electrodeposition of CdSe Nanoparticles. For the electrodeposition of ∼25 nm CdSe, a 0.1 M $CdCl_2$ (>99.0%, Fluka), 0.2 mM SeO_2 (>99.9%, Aldrich), and 0.1 M Na_2SO_4 (>99.0%, Sigma-Aldrich) aqueous solution at a pH of 2.7, controlled by the addition of 1 N HCl (Samchun), was prepared. Then, −0.7 V vs SCE was applied to the CdS-decorated TiO_2 nanotube array sample for 2 h, followed by annealing at 150 °C for 30 min in air.[20]

Fabrication of Photoelectrode/Dye-Sensitized Solar Cell (DSSC) Tandem Structure. The DSSC was prepared according to the following procedure. The clean FTO glass substrate was immersed for 30 min at 80 °C in a 40 mM titanium tetrachloride ($TiCl_4$, Aldrich) aqueous solution before being rinsed with ethanol. The nanocrystalline transparent TiO_2 electrode was doctor-bladed on the pretreated FTO glass substrate and sintered at 550 °C for 30 min. To improve the connectivity between the TiO_2 nanoparticles, we treated the electrode in a 40 mM $TiCl_4$ aqueous solution at 80 °C for 30 min and sintered again at 550 °C for 30 min. Once the electrode cooled, it was immersed in a 0.3 mM solution of N719 dye in ethanol for 18 h. The counter electrode was prepared simultaneously by spin coating using a solution of 10 mM H_2PtCl_6 (Aldrich) in isopropyl alcohol on the clean FTO glass substrate and sintered at 450 °C for 30 min. The photoanode and the counter electrode were assembled using a 60 μm thick Surlyn spacer and filled with an iodine/triiodide redox couple electrolyte. For the tandem cell, photoanode and DSSC were firmly secured each other using clip then electrically connected via copper conducting tape.

Characterization Methods. To examine the sample morphology, field emission scanning electron microscopy (FE-SEM, JSM-7000F, Japan) and transmission electron microscopy (HRTEM, JEM-3010, Japan) were used. X-ray diffraction measurements were performed to observe the crystalline phase with a Siemens diffractometer D500/5000 in Bragg−Brentano geometry under Cu K radiation. Additionally, the optical properties were investigated using a UV−vis spectrophotometer (UV-2401 PC, Shimadzu).

Photoelectrochemical Measurements. The electrochemical properties were investigated using an electrochemical workstation (CH Instruments, CHI 608C) with a three-electrode configuration: Pt wire as a counter electrode and $Hg/HgSO_4$ as a reference electrode in a 0.35 M Na_2SO_3 and 0.24 M Na_2S aqueous solution as an electrolyte. A H-type quartz cell was used as a reactor, the photoanode was placed outside of the reactor and contact with the electrolyte through a hole on the side wall of the reactor. Linear sweep voltammetry was

DOI: 10.1021/acsami.5b04521
ACS Appl. Mater. Interfaces 2015, 7, 18429−18434

performed at a scan rate of 20 mV/s. The working electrode was illuminated with a 150 W xenon lamp-based solar simulator (PECCELL, Yokohama, Japan, PEC-L01:100 mW/cm^2), and the light intensity was calibrated using a silicon reference cell (Fraunhofer ISE, Certificate No. C-ISE269). The measured light irradiance was 100 mW/cm^2. For characterization of the dye-sensitized solar cell, photocurrent density-photovoltage (J–V) was measured under AM1.5 simulated solar light irradiation using a 300 W xenon lamp (Newport) calibrated using a standard Si solar cell.

Quantitative Measurement of Hydrogen. In the tandem cell, the hydrogen gas evolved from the surface of the Pt cathode and was collected in a sealed quartz tube during photoelectrochemical reaction. The generated hydrogen gas was quantitatively measured using a gas chromatograph equipped with a thermal conductivity detector. Before the H_2 generation experiment, 1 mL of the gas in the closed H-type quartz reactor filled with nitrogen gas was examined to confirm that there is no oxygen or hydrogen. Hydrogen gas was generated under the light irradiation. Then, 1 ml of the sample gas was collected by a gastight syringe from the reactor and examined every 20 min during the 2 h experiment. The number of moles of gas product was calculated from the ideal gas law, and GC results were used to calculate the volume of the hydrogen gas in the mixture

RESULTS AND DISCUSSION

The vertically aligned 1D TiO_2 nanorod arrays were synthesized directly on a FTO substrate using the hydrothermal method, as described in the Experimental Section. The morphologies of the synthesized TiO_2 nanorod arrays are shown in Figure S1. Figure S1a,b shows typical top-view and cross-sectional SEM images of the TiO_2 nanorods. The shape of the nanorod array is square with a diameter of approximately 100 nm. The top surfaces of the nanorods contain many step edges, whereas the side surfaces are smooth. Figure S1c,d shows an HR-TEM image and the corresponding selected area electron diffraction (SAED) pattern of the TiO_2 nanorods, respectively. TiO_2 nanorods have lattice fringes with interplanar distances of d_{110} = 0.32 nm and d_{001} = 0.29 nm because the TiO_2 nanorods grow along the (110) plane with a [001] direction, which can be attributed to the tetragonal rutile phase (JCPDS card no. 21-1276). According to previous reports, the unique growth orientation of the TiO_2 nanorod arrays on a FTO substrate is caused by the (001) facet, which is considerably more reactive than other facets.[21,22]

The morphologies of the rectangular TiO_2 nanotube arrays, which were synthesized by chemical etching using the TiO_2 nanorod arrays, are shown in Figure S2 as a function of the acid treatment time. It has been reported that TiO_2 dissolves in HF solution, forming TiF_6^{2-} ion in solution.[23] For the kinetic control of the dissolution, certain concentration of HCl was provided as well as heat.[19] In the case of the reaction for this morphology, the dissolution rate of the TiO_2 nanorod arrays on the FTO substrate in combination with the long-axis direction is much faster than the side wall direction.[9] The TiO_2 nanorods transform into nanotubes with increasing etching reaction times. After etching for 1 h under the specified acidic conditions (see Experimental Section), the surface of the nanorod-shaped TiO_2 arrays start to roughen. This observation indicates that the nanorods have been partially dissolved by the strong acidic solution. When the etching reaction was extended to 3 h, the TiO_2 nanorod arrays were transformed partially to the rectangular nanotube structure. After a 5 h etching period, most of the nanorod arrays adopted the nanotube morphology. The chemical etching process did not affect the length of the arrays up to 3 h, but it made the arrays shorter and more irregular after 5 h of etching.

To expand the available wavelength region of solar light, CdS/CdSe nanoparticles with low bandgap energies were cosensitized on the surface of TiO_2 nanorods and nanotubes. The electrochemically synthesized CdS and CdSe nanoparticles on the TiO_2 surface have diameters of approximately 100 nm (Figure 2a) and 30 nm (Figure 2b), respectively. After the

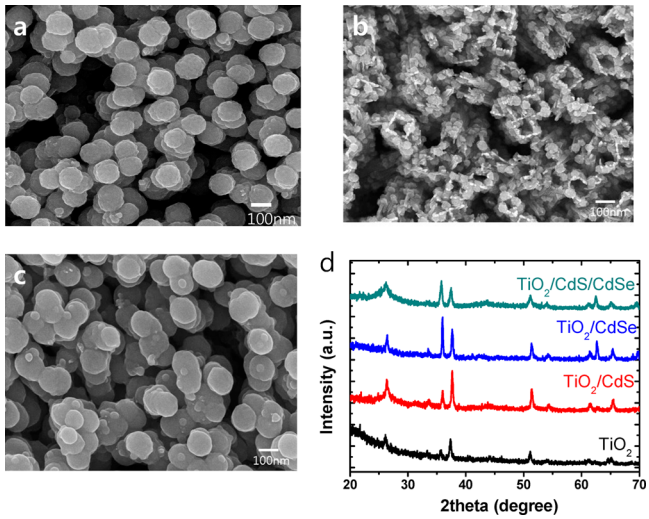

Figure 2. FE-SEM images of the composite composed of acid treated TiO_2 for 3 h with (a) electrodeposited CdS for 1000 s, (b) electrodeposited CdSe for 2 h, and (c) CdS and CdSe together for 1000 s and 2 h, respectively. (d) XRD patterns of the chemically etched TiO_2 nanotubes or its composite with CdS and/or CdSe.

deposition of CdS and then CdSe, we could observe CdSe nanoparticles decorating the CdS core morphology (Figure 2c). Figure 3 shows SEM images of the CdS@CdSe nanoparticles

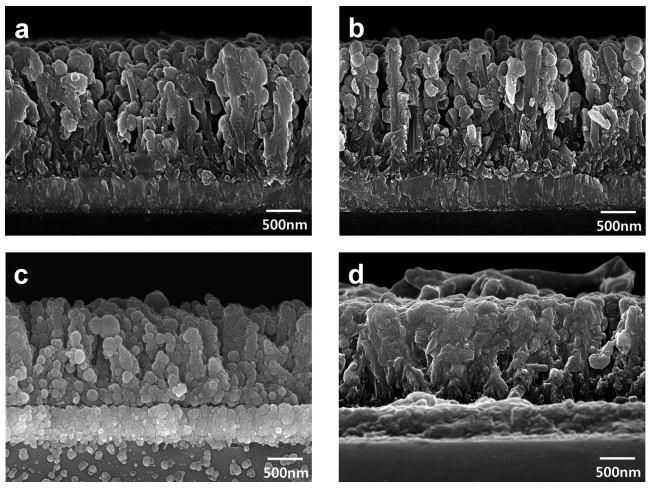

Figure 3. FE-SEM images of the CdS and CdSe codeposited (a) TiO_2 nanorod arrays, and the acid treated TiO_2 nanotube arrays for (b) 1, (c) 3, and (d) 5 h.

deposited onto TiO_2 nanotube arrays with different etching reaction times. In the case of as-synthesized (Figure 3a) or 1 h etched (Figure 3b) TiO_2 samples, which have a nanorod morphology, the deposited CdS@CdSe aggregated considerably over the whole TiO_2 nanorod arrays. However, when the CdS@CdSe were deposited on the TiO_2 nanotube arrays prepared by 3 h of etching, more uniform CdS@CdSe

DOI: 10.1021/acsami.5b04521
ACS Appl. Mater. Interfaces 2015, 7, 18429–18434

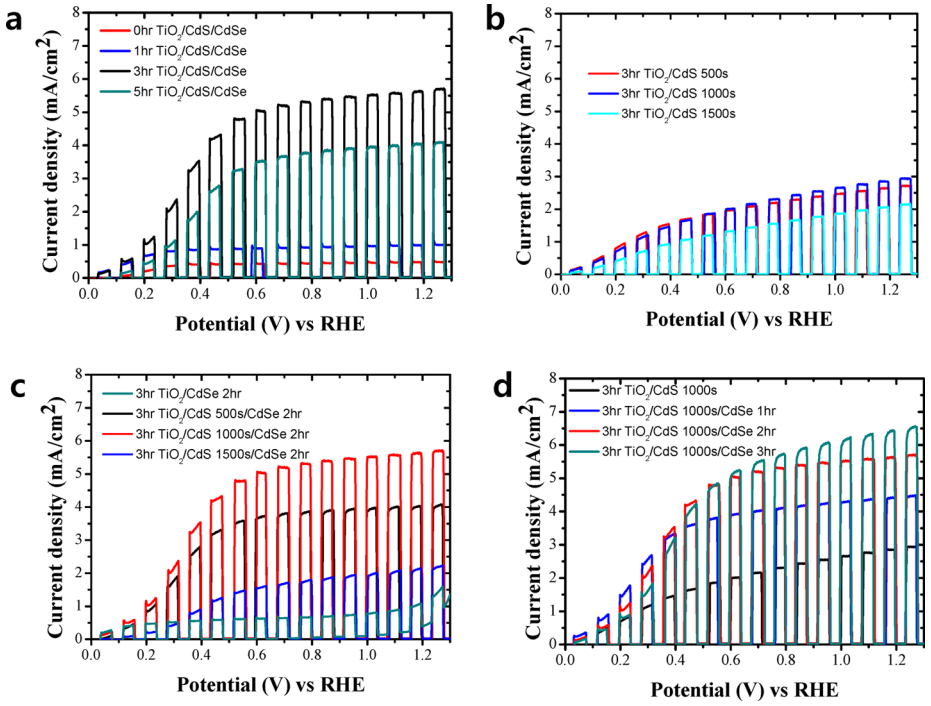

Figure 4. Photoelectrochemical $J-V$ curves of (a) CdS/CdSe decorated TiO_2 nanorod arrays as a function of etching reaction time, (b) TiO_2 nanotube arrays (3 h etching)@CdS composite with different deposition times of CdS, (c) TiO_2 nanotube arrays (3 h etching)@CdS@CdSe composite with different deposition times of CdS and fixed deposition time of CdSe, and (d) TiO_2 nanotube arrays (3 h etching)@CdS@CdSe composite with fixed electrodeposition time of CdS (1000 s), but different electrodeposition times of CdSe.

nanoparticles decorated the TiO_2 nanotubes, as shown in Figure 3c. Presumably, the nanotube morphology with an enlarged surface area may be a better scaffold for the CdS@CdSe decoration using the electrodeposition method.[24] However, as we expected from Figure S2, the TiO_2 nanotube arrays etched for 5 h and decorated with CdS@CdSe exhibited a very poor morphology because of the almost broken nanotubular structures. As confirmed by energy-dispersive X-ray spectroscopy (EDS) of the TiO_2 nanotube arrays@CdS@CdSe with 3 h of etching (Figure S3), the sensitizers of CdS@CdSe were well distributed inside the TiO_2 film.

The PEC properties ($J-V$ curves) of the TiO_2 nanotube arrays@CdS@CdSe photoanodes were investigated. First, the effect of the etching process on the PEC properties of the pure 1D TiO_2 nanorod arrays was studied, as shown in Figure S4. In general, the photocurrent generation of a photoanode may be influenced by light absorption, charge separation, and surface charge transfer.[25,26] Although the tubular samples showed a lower light absorbance than that of the rod samples (Figure S5a), the TiO_2 nanotube arrays after etching showed a considerably higher photocurrent density than the as-synthesized TiO_2 nanorod arrays. This result may be because the different nanostructures of the photoanode with an enhanced surface area lead to high charge separation and transfer efficiencies. To investigate the effectiveness of the etching process on the $J-V$ curves of the 1D TiO_2 arrays@CdS@CdSe composite materials, we prepared CdS@CdSe on 1D TiO_2 nanorod or nanotube arrays as a function of the etching time and measured their $J-V$ curves under light chopping conditions, as shown in Figure 4a. Note that CdS and CdSe nanoparticles were electrodeposited for 1000 s and 2 h, respectively, which were the optimum conditions. Similar to the $J-V$ curves of the pure TiO_2 photoanodes, the nanotube morphologies decorated with CdS@CdSe exhibited a strong photocurrent enhancement. When the as-synthesized TiO_2 nanorod arrays were decorated with CdS@CdSe, the saturated photocurrent density was approximately 0.5 mA/cm^2. By contrast, when we employed TiO_2 nanotube arrays prepared from 3 h of etching, the composite material showed a greatly enhanced photocurrent density, reaching approximately 5.7 mA/cm^2. Although this photocurrent density is not comparable with those of previous reports employing TiO_2 and CdS or CdSe, note that our samples are semitransparent (Figure S5b) for further use in tandem PEC cells. This result also confirms that the nanotube morphology leads to an effective charge separation between the TiO_2 host and CdS@CdSe guest materials.

To optimize the CdS@CdSe sensitizer on 3 h etched TiO_2 nanotube arrays, the electrodeposition conditions of CdS and CdSe were varied. First, the electrodeposition time for CdS was varied from 0, 500, 1000, and 1500 s. As shown in Figure 4b, the photocurrent density increased gradually in accordance with the deposition time and reached a maximum value of approximately 3 mA/cm^2 when the CdS was deposited for 1000 s. The CdS deposition increased the photocurrent density, but the CdS decoration for 1500 s resulted in an abrupt decrease in the photocurrent density, which is one-third of that at 1000 s. Presumably, the thicker the CdS nanoparticle film with many grain boundaries may induce severe electron/hole recombination, resulting in such a poor electrochemical photocurrent density. Second, the amount of CdSe was further optimized by changing the electrodeposition time on the TiO_2 sample, which was prepared using 3 h etched TiO_2 nanotube arrays and 1000 s electrodeposition of CdS. The electrodeposition time for CdSe was controlled from 1 to 3 h because the kinetics of the electrochemical reaction for the CdSe deposition was much slower than in the CdS case, and a few tens of nanometer sized particles could be formed.[18] CdSe has a

DOI: 10.1021/acsami.5b04521
ACS Appl. Mater. Interfaces 2015, 7, 18429−18434

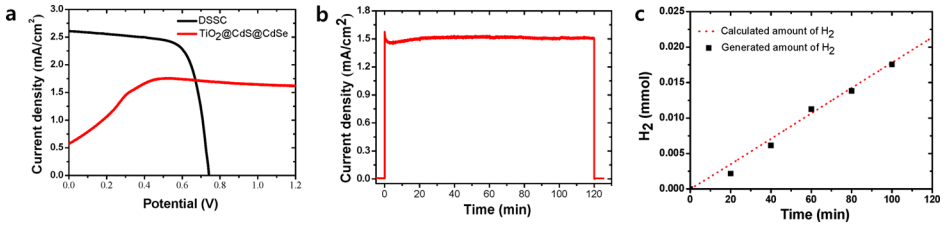

Figure 5. (a) $J-V$ curves of the best TiO_2 nanotube arrays@CdS@CdSe composite electrode and dye-sensitized solar cell in the two-electrode system, (b) J-t curve of the tandem cell, and (c) calculated and generated amount of hydrogen gas from the tandem cell.

much lower bandgap of 1.7 eV and efficiently enhanced the photocurrent density by extending the light absorption range to a wavelength of ~720 nm (Figure S6a). As shown in Figure 4d, the additional CdSe decoration improved the photocurrent density to 6.5 mA/cm^2, which is at least 1.5 times higher than without CdSe decoration. However, when a longer electrodeposition time was used that exceeds this optimal condition for CdSe, a lower photocurrent density was observed around the applied potential of less than 0.5 V vs RHE. It is likely that this phenomenon is also attributed to the fact that electrons generated by the thick CdSe films could not be transferred into the CdS effectively. Interestingly, as shown in Figure 4a, TiO_2 nanotube arrays@CdSe only exhibited a photocurrent density of less than 1 mA/cm^2. This means that direct contact between the TiO_2 nanotube arrays and the CdSe nanoparticles was not effective in improving the photocurrent density, even though there was no theoretical energy barrier between their interfaces. However, inserting a CdS material between the CdSe and TiO_2 forming proved to be more than adequate to increase the photocurrent density.

To realize spontaneous solar water splitting from a PEC/solar cell tandem configuration, we need a highly transparent photoelectrode located in the front side of a solar cell. Figure S5b provides strong evidence for the effectiveness of the etching process in enhancing the transparency of the 1D TiO_2 nanotube arrays. The as-prepared 1D TiO_2 nanorod arrays exhibited a transparency of approximately 30% at a wavelength of 700 nm. However, the transparency of the TiO_2 electrode was improved to approximately 60% after being etched for 3 h. Even after coating the TiO_2 nanotube arrays with CdS and CdS@CdSe, the composite materials exhibited a transparency of approximately 50% at a wavelength of 1000 nm (Figure S6b). The cosensitized TiO_2 nanotube arrays, prepared under optimized sensitization conditions to provide the best photocurrent density, were used to fabricate an unassisted PEC hydrogen generation device with the help of a DSSC. Before we fabricated the tandem cell with the DSSC, the PEC properties of the electrochemical system composed of the cosensitized TiO_2 nanotube arrays and the platinum cathode were investigated using a two-electrode system, and the photovoltaic properties of the DSSC placed behind the composite nanomaterial were also tested (Figure 5a). The operating point of the unassisted PEC hydrogen generation device is the intersection on the $J-V$ curves for each of those two devices, at 0.67 V.[27] Each of those devices were stacked up and copper tape applied to connect each other's conductive side between the composite photoanode material and the DSSC cathode. The tandem device showed a photocurrent density of 1.7 mA/cm^2 without any applied potential. This device was utilized to generate hydrogen gas by light irradiation for 2 h (Figure 5b). In this experiment, the samples showed very stable photocurrent densities without serious current decay, and there was no oxygen gas generation because the sulfide behaved as a sacrificial oxidizing agent, which was oxidized instead of water to prevent anodic dissolution of the cadmium-based materials. Therefore, only hydrogen gas was evolved in the system. Figure 5b shows the $I-t$ curve for the tandem cell during the PEC hydrogen generation reaction, and the generated hydrogen gas is equilibrant with the calculated value from the photocurrent. On the basis of the photocurrent density and the volume of the generated hydrogen gas, we confirmed that the faradaic efficiency for hydrogen generation was approximately 100%. On the basis of the above results, calculated solar to hydrogen efficiency was about 2.1% (calculation details in Supporting Information).

CONCLUSION

The present results show that the controlled chemical etching reaction (e.g., 3 h) can transform TiO_2 nanorods into nanotubes, which can enhance light transmission dramatically. For efficient visible light harvesting, CdS and CdSe particles were codeposited onto the TiO_2 nanotubes using electrodeposition. The TiO_2 nanotubes were decorated well by the CdS and CdSe composite particles. The electrode, which was composed of TiO_2 nanotube arrays@CdS@CdSe, exhibited enhanced photoelectrochemical properties, as well as excellent transparency to solar light. The optimized conditions for the deposition of CdS and CdSe were 1000 s and 3 h, respectively. With the improved optical and photoelectrochemical properties of the composite materials, a sandwich-type tandem cell with a rear DSSC was fabricated for the generation of hydrogen gas without any applied bias. The tandem PEC cell showed a photocurrent of 1.7 mA/cm^2 under 100 mW/cm^2 with no bias.

ASSOCIATED CONTENT

Supporting Information

The Supporting Information is available free of charge on the ACS Publications website at DOI: 10.1021/acsami.5b04521.

Additional SEM and TEM images, EDS spectra, additional photoelectrochemical $J-V$ curves, UV–vis absorption and transmission spectra, and the DSSC cell performance (PDF)

AUTHOR INFORMATION

Corresponding Author

*E-mail: lutts@yonsei.ac.kr.

Notes

The authors declare no competing financial interest.

ACKNOWLEDGMENTS

This work was supported by the NRF of Korea Grant funded by the Ministry of Science, ICT & Future Planning (NRF-2013R1A2A1A09014038, 2011-0030254).

DOI: 10.1021/acsami.5b04521
ACS Appl. Mater. Interfaces 2015, 7, 18429–18434

REFERENCES

(1) Fujishima, A.; Honda, K. Electrochemical Photolysis of Water at a Semiconductor Electrode. *Nature* **1972**, *238*, 37−38.

(2) Beranek, R.; Tsuchiya, H.; Sugishima, T.; Macak, J. M.; Taveira, L.; Fujimoto, S.; Kisch, H.; Schmuki, P. Enhancement and Limits of the Photoelectrochemical Response from Anodic TiO_2 Nanotubes. *Appl. Phys. Lett.* **2005**, *87*, 243114.

(3) Lin, C.; Lu, Y.; Hsieh, C.; Chien, S. Surface Modification of Highly Ordered TiO_2 Nanotube Arrays for Efficient Photoelectrocatalytic Water Splitting. *Appl. Phys. Lett.* **2009**, *94*, 113102.

(4) Wolcott, A.; Smith, W. A.; Kuykendall, T. R.; Zhao, Y.; Zhang, J. Z. Photoelectrochemical Water Splitting Using Dense and Aligned TiO_2 Nanorod Arrays. *Small* **2009**, *5*, 104−111.

(5) Li, Q.; Lu, G. Controlled Synthesis and Photocatalytic Investigation of Different-Shaped One-Dimensional Titanic Acid Nanomaterials. *J. Power Sources* **2008**, *185*, 577−583.

(6) Lei, Y.; Zhang, L. D.; Meng, G. W.; Li, G. H.; Zhang, X. Y.; Liang, C. H.; Chen, W.; Wang, S. X. Preparation and Photoluminescence of Highly Ordered TiO_2 Nanowire Arrays. *Appl. Phys. Lett.* **2001**, *78*, 1125−1127.

(7) Lee, J. C.; Park, K. S.; Kim, T. G.; Choi, H. J.; Sung, Y. M. Controlled Growth of High-quality TiO_2 Nanowires on Sapphire and Silica. *Nanotechnology* **2006**, *17*, 4317−4321.

(8) Liu, B.; Aydil, E. S. Growth of Oriented Single-Crystalline Rutile TiO_2 Nanorods on Transparent Conducting Substrates for Dye-Sensitized Solar Cells. *J. Am. Chem. Soc.* **2009**, *131*, 3985−3990.

(9) Liu, L.; Qian, J.; Li, B.; Cui, Y.; Zhou, X.; Guo, X.; Ding, W. Fabrication of Rutile TiO_2 Tapered Nanotubes with Rectangular Cross-Sections via Anisotropic Corrosion Route. *Chem. Commun.* **2010**, *46*, 2402−2404.

(10) Cheng, S.; Fu, W.; Yang, H.; Zhang, L.; Ma, J.; Zhao, H.; Sun, M.; Yang, L. Photoelectrochemical Performance of Multiple Semiconductors (CdS/CdSe/ZnS) Cosensitized TiO_2 Photoelectrodes. *J. Phys. Chem. C* **2012**, *116*, 2615−2621.

(11) Lee, Y.-L.; Chi, C.-F.; Liau, S.-Y. CdS/CdSe Co-Sensitized TiO_2 Photoelectrode for Efficient Hydrogen Generation in a Photoelectrochemical Cell. *Chem. Mater.* **2010**, *22*, 922−927.

(12) Zhang, Q.; Guo, X.; Huang, X.; Huang, S.; Li, D.; Luo, Y.; Shen, Q.; Toyoda, T.; Meng, Q. Highly Efficient CdS/CdSe-Sensitized Solar Cells Controlled by the Structural Properties of Compact Porous TiO_2 Photoelectrodes. *Phys. Chem. Chem. Phys.* **2011**, *13*, 4659−4667.

(13) Lee, Y.-L.; Lo, Y.-S. Highly Efficient Quantum-Dot-Sensitized Solar Cell Based on Co-Sensitization of CdS/CdSe. *Adv. Funct. Mater.* **2009**, *19*, 604−609.

(14) Acharya, K. P.; Hewa-Kasakarage, N. N.; Alabi, T. R.; Nemitz, I.; Khon, E.; Ullrich, B.; Anzenbacher, P.; Zamkov, M. Synthesis of PbS/TiO_2 Colloidal Heterostructures for Photovoltaic Applications. *J. Phys. Chem. C* **2010**, *114*, 12496−12504.

(15) Lee, H.; Leventis, H. C.; Moon, S.-J.; Chen, P.; Ito, S.; Haque, S. A.; Torres, T.; Nüesch, F.; Geiger, T.; Zakeeruddin, S. M.; Grätzel, M.; Nazeeruddin, Md. K. PbS and CdS Quantum Dot-Sensitized Solid-State Solar Cells: "Old Concepts, New Results. *Adv. Funct. Mater.* **2009**, *19*, 2735−2742.

(16) Ratanatawanate, C.; Tao, Y.; Balkus, K. J., Jr Photocatalytic Activity of PbS Quantum Dot/TiO_2 Nanotube Composites. *J. Phys. Chem. C* **2009**, *113*, 10755−10760.

(17) Cho, C.-Y.; Lee, J.; Lee, D. C.; Moon, J. H. Uniform Decoration of CdS Nanoparticles on TiO_2 Inverse Opals for Visible Light Photoelectrochemical Cell. *Electrochim. Acta* **2015**, *166*, 350−355.

(18) Ding, D.; Chen, Y.; Lv, P.; Yao, H.; Mu, Y.; Su, S.; Zhang, X.; Zhou, L.; Fu, W.; Yang, H. Efficient Improvement of Photoelectrochemical Activity for Multiple Semiconductor (CdS/PbS/ZnS) Co-sensitized TiO_2 Photoelectrodes by Hydrogen Treatment. *RSC Adv.* **2015**, *5*, 6462−6469.

(19) Bright, E.; Readey, D. W. Dissolution Kinetics of TiO_2 in HF-HCl Solutions. *J. Am. Ceram. Soc.* **1987**, *70*, 900−906.

(20) Yang, L.; Luo, S.; Liu, R.; Cai, Q.; Xiao, Y.; Liu, S.; Su, F.; Wen, L. Fabrication of CdSe Nanoparticles Sensitized Long TiO_2 Nanotube Arrays for Photocatalytic Degradation of Anthracene-9-carbonxylic Acid under Green Monochromatic Light. *J. Phys. Chem. C* **2010**, *114*, 4783−4789.

(21) Yang, H. G.; Sun, C. H.; Qiao, S. Z.; Zou, J.; Liu, G.; Smith, S. C.; Cheng, H. M.; Lu, G. Q. Anatase TiO_2 Single Crystals with a Large Percentage of Reactive Facets. *Nature* **2008**, *453*, 638−641.

(22) Feng, X.; Shankar, K.; Varghese, O. K.; Paulose, M.; Latempa, T. J.; Grimes, C. A. Vertically Aligned Single Crystal TiO_2 Nanowire Arrays Grown Directly on Transparent Conducting Oxide Coated Glass: Synthesis Details and Applications. *Nano Lett.* **2008**, *8*, 3781−3786.

(23) Macák, J. M.; Tsuchiya, H.; Schmuki, P. High-Aspect-Ratio TiO_2 Nanotubes by Anodization of Titanium. *Angew. Chem., Int. Ed.* **2005**, *44*, 2100−2102.

(24) Banerjee, S.; Mohapatra, S. K.; Das, P. P.; Misra, M. Synthesis of Coupled Semiconductor by Filling 1D TiO_2 Nanotubes with CdS. *Chem. Mater.* **2008**, *20*, 6784−6791.

(25) Dotan, H.; Sivula, K.; Gratzel, M.; Rothschild, A.; Warren, S. C. Probing the Photoelectrochemical Properties of Hematite (α-Fe_2O_3) Electrodes Using Hydrogen Peroxide as a Hole Scavenger. *Energy Environ. Sci.* **2011**, *4*, 958−964.

(26) Chen, Z.; Jaramillo, T. F.; Deutsch, T. G.; Kleiman-Shwarsctein, A.; Forman, A. J.; Gaillard, N.; Garland, R.; Takanabe, K.; Heske, C.; Sunkara, M.; McFarland, E. W.; Domen, K.; Miller, E. L.; Turner, J. Accelerating Materials Development for Photoelectrochemical Hydrogen Production: Standards for Methods, Definitions, and Reporting Protocols. *J. Mater. Res.* **2010**, *25*, 3−16.

(27) Abdi, F. F.; Han, L.; Smets, A. H. M.; Zeman, M.; Dam, B.; van de Krol, R. Efficient Solar Water Splitting by Enhanced Charge Separation in a Bismuth Vanadate-Silicon Tandem Photoelectrode. *Nat. Commun.* **2013**, *4*, 2195.

DOI: 10.1021/acsami.5b04521
ACS Appl. Mater. Interfaces 2015, 7, 18429−18434